On-Surface Synthesis of BN-Substituted Heteroaromatic Networks

Carlos Sánchez-Sánchez,[*,†] Sebastian Brüller,[‡] Hermann Sachdev,[‡,§] Klaus Müllen,[‡] Matthias Krieg,[∥] Holger F. Bettinger,[∥] Adrien Nicolaï,[⊥] Vincent Meunier,[⊥] Leopold Talirz,[†] Roman Fasel,[†,#] and Pascal Ruffieux[*,†]

[†]Empa, Swiss Federal Laboratories for Materials Science and Technology, Überlandstrasse 129, CH-8600 Dübendorf, Switzerland, [‡]Max Planck Institut for Polymer Research, Ackermannweg 10, 55128 Mainz, Germany, [§]Mechanische Verfahrenstechnik, TU Kaiserslautern, Gottlieb Daimler Straße 44, 67663 Kaiserslautern, Germany, [∥]Institut für Organische Chemie, Universität Tübingen, Auf der Morgenstelle 18, 72076 Tübingen, Germany, [⊥]Department of Physics, Rensselaer Polytechnic Institute, Troy, New York 12180, United States, and [#]Department of Chemistry and Biochemistry, University of Bern, Freiestrasse 3, CH-3012 Bern, Switzerland

ABSTRACT We report on the bottom-up fabrication of BN-substituted heteroaromatic networks achieved by surface-assisted polymerization and subsequent cyclodehydrogenation of specifically designed BN-substituted precursor monomers based on a borazine core structural element. To get insight into the cyclodehydrogenation pathway and the influence of molecular flexibility on network quality, two closely related precursor monomers with different degrees of internal cyclodehydrogenation have been employed. Scanning tunneling microscopy shows that, for both monomers, surface-assisted cyclodehydrogenation allows for complete monomer cyclization and the formation of covalently interlinked BN-substituted polyaromatic hydrocarbon networks on the Ag(111) surface. In agreement with experimental observations, density functional theory calculations reveal a significantly lower energy barrier for the cyclodehydrogenation of the conformationally more rigid precursor monomer, which is also reflected in a higher degree of long-range order of the obtained heteroaromatic network. Our proof-of-concept study will allow for the fabrication of atomically precise substitution patterns within BNC heterostructures.

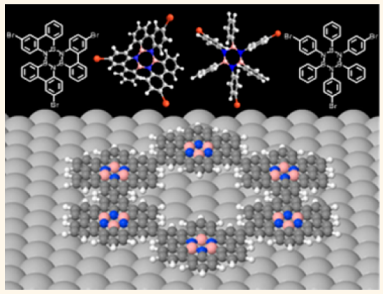

KEYWORDS: graphene · hexagonal boron nitride · bottom-up · cyclodehydrogenation · covalent network · scanning tunneling microscopy · density functional theory

Surface-assisted cyclodehydrogenation (SAC) has recently been identified as a very promising route to the fabrication of novel (macro)molecular structures which are otherwise not available *via* traditional solution-based chemistry.[1] This method, based on the exploitation of specific catalytic properties of metal surfaces, has led to more efficient synthetic pathways or even to new molecular species. Fabrication of fullerenes,[2] azafullerenes,[2,3] nanodomes,[4−6] and nanographenes[6−9] *via* SAC has been reported in the last years. Although mostly carbon-based and nitrogen-doped structures have been fabricated so far, there are no inherent limitations for this strategy to be extended to more complex systems, as far as the necessary precursor monomers can be synthesized.[10] The method can thus be envisaged as a powerful tool for the fabrication of complex heterostructures where atomic precision is required. One example is the challenging fabrication of in-plane hexagonal boron−nitride−carbon (*h*-BNC) heterostructures.[11] This hybrid material presents high potential in different technological fields such as electronics, where a band gap opening in graphene is needed for the realization of efficient switching devices,[12−14] or nonlinear optics,[15] among others. Different strategies have been explored in the past decade, mainly focused on sequential CVD growth or on top-down patterning.[16−23] However, as inherent to methods based on these approaches, the resulting structures lack the atomic precision necessary to fully control and reproduce the predicted properties. Finding a new route to fabricate *h*-BNC heterostructures with atomically precise BN/C boundaries would significantly improve their applicability in future technologies. Recently, an important step forward has been achieved by M. Krieg *et al.*, who have successfully synthesized a hexa-*peri*-hexabenzocoronene (HBC) with a central borazine core ("BN substituted HBC",

* Address correspondence to carlos.sanchez@empa.ch, pascal.ruffieux@empa.ch.

Received for review June 25, 2015 and accepted August 17, 2015.

Published online August 17, 2015
10.1021/acsnano.5b03895

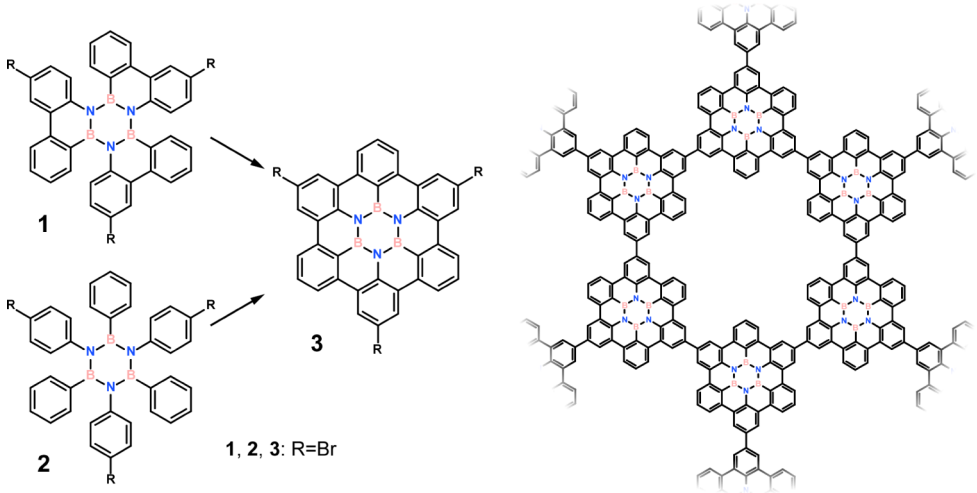

Figure 1. Schematic representation of monomers 1 and 2 used in the experiments and the expected final product upon complete cyclodehydrogenation (BN-HBC, 3). The 3-fold bromine substitution furthermore allows for the formation of 2D networks *via* aryl−aryl coupling as indicated in the right panel.

BN-HBC) *via* thermolysis of a tailored precursor monomer.[24] However, a tetraazatetraborocine derivative is simultaneously formed in this reaction, BN-HBC being the minority product.

In this work, we show that structural accuracy and high efficiency can be achieved *via* SAC. Furthermore, we combine SAC with on-surface aryl−aryl coupling to fabricate not only 0D but also 2D structures. Specifically, we show how surface-assisted cyclodehydrogenation of two distinct borazine-based precursor monomers, 2,12,22-tribromo-tri(*o*,*o*′-biphenylyl)borazine[25−27] (**1**) and 1,3,5-tri(4-bromophenyl)-2,4,6-triphenylborazine (**2**) (Figure 1), on a clean Ag(111) surface under UHV conditions allows for the formation of atomically precise BN-HBC. The two different precursor monomers **1** and **2** have been chosen for three reasons: first, to shed light on the cyclodehydrogenation pathway as monomer **1** is a partially cyclodehydrogenated analogue of **2** (closer to planarity and stiffer); second, to allow for surface-assisted aryl−aryl coupling into 2D polymer networks utilizing their 3-fold Br-substituents; and third, to explore the impact of monomer flexibility on the quality of the covalently bonded *h*-BNC hybrid networks. From our results, we obtain a detailed picture on the SAC pathway of both precursor monomers. Furthermore, clear evidence of the importance of monomer flexibility with respect to the resulting network quality is presented. Our proof-of-concept study opens a door toward the design and synthesis of atomically precise BN-substituted heteroaromatics and derived 1- or 2-D networks with potential applications in electronics and optics.

RESULTS

Deposition of the "partially pre-planarized" precursor monomer **1** with biphenyl-type interlinked B- and N- aryl substituents under UHV conditions on the clean Ag(111) surface held at 425 K yields flower-like structures as shown in Figure 2a. In this small-scale STM image, the presence of triangular building blocks with three inner maxima and an apparent height of 1.8 Å can be discerned. These features are in agreement with the expected shape of individual precursor monomers, where the three maxima correspond to the tilting of the three *o*,*o*′-biphenylyl units (from now on called "wings") due to steric hindrance between the inner hydrogen atoms. Analysis of the relative position of the maxima with respect to the intermolecular bonding directions rationalizes a molecular conformation where the benzene rings bonded to the N atoms lie closer to the surface, forcing the other ones in the same "wing" to protrude away from it. The separation between consecutive molecules is larger than the expected value for covalently bonded molecules (∼15.0 *vs* 12.6 Å, monomer center-to-center distance). However, it is well established that a temperature of 425 K is high enough to induce the dehalogenation of the bromine atoms in organic molecules when deposited on Ag(111), due to the catalytic activity of the metallic surface.[28] Thus, the most plausible explanation is that a silver adatom-based organometallic self-assembled superstructure has been formed, as reported earlier for the case of dimethylmethylene-bridged triphenylamine (DTPA) on Ag(111).[29] Regarding the number of monomers per flower-like structure, a coexistence of pentamers, hexamers, heptamers, and higher order rings is observed. As shall be discussed later on, this is associated with the flexibility of the precursor monomers and the type of bonding (organometallic C−M−C bond between neighboring molecules *vs* intermolecular C−C covalent bond, the first one being more flexible).

Postannealing the surface at 475 K results in a decrease of the intermolecular distances from 15.0 to 12.9 Å (Figure 2b). This value is in good agreement with

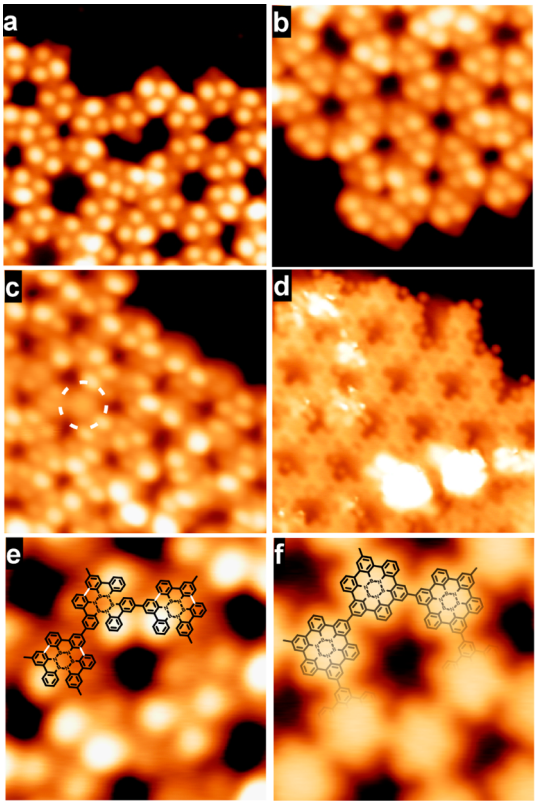

Figure 2. STM images of monomer 1 deposited on the clean Ag(111) surface after annealing at 425 K (a), 475 K (b), 525 K (c), and 575 K (d). (a) Organometallic self-assembled superstructure (100 Å × 100 Å, *I* = 150 pA, *U* = −1.5 V). (b) Covalent network (100 Å × 100 Å, *I* = 50 pA, *U* = −1.5 V). (c) Partial cyclodehydrogenation of the monomers. A fully cyclodehydrogenated monomer is highlighted by the dashed white circle (100 Å × 100 Å, *I* = 150 pA, *U* = −1.5 V). (d) Fully cyclodehydrogenated network (100 Å × 100 Å, *I* = 100 pA, *U* = −1.5 V). (e) High-resolution STM image of the partially cyclodehydrogenated network after annealing to 525 K. A schematic molecular model has been superimposed. C−C bonds formed *via* SAC are highlighted in white (42 Å × 42 Å, *I* = 150 pA, *U* = −1.5 V). (f) High-resolution STM image of the fully cyclodehydrogenated network obtained after annealing at 575 K. Good agreement with the scaled schematic molecular model is observed (42 Å × 42 Å, *I* = 150 pA, *U* = −1.5 V).

the expected distance of covalently bonded monomers, thus indicating a transition from an organometallic self-assembled superstructure to a covalent network. Molecules preserve the three internal maxima with the same apparent height, indicating that no cyclodehydrogenation has taken place up to this temperature. Additionally, prevalence for the formation of hexamers in detriment to other order pores is observed, due to the increased rigidity/directionality of the covalent *vs* organometallic bond.

Further annealing to 525 K induces a change in molecular appearance. As evidenced in Figure 2c, molecules with three, two, one, or even no internal maxima coexist. For instance, a completely flat monomer is highlighted by a white dashed circle. This monomer presents a lower apparent height of 1.3 Å. This can be understood in terms of cyclodehydrogenation of the molecule: if neighboring H atoms from different molecular "wings" are cleaved, steric hindrance is drastically reduced allowing for the formation of a new C−C bond and thus flattening the two bora-aza-phenenthrene units by interlinkage. This will automatically translate into a decrease in the apparent height. Figure 2e shows a small-scale STM image where partially cyclodehydrogenated monomers are visible. A schematic model of the molecular network is superimposed for comparison. The newly formed bonds are highlighted in white. If these bonds are included, a good agreement between model and experiment is obtained. The symmetry of the molecules does not indicate any specific intramolecular cyclodehydrogenation sequence, thus suggesting a random process as it is confirmed by a statistical analysis of STM images.

Finally, annealing to 575 K fully cyclodehydrogenates the molecular network (Figure 2d). Monomers present a homogeneous appearance rather than the three internal maxima exhibited before. The apparent height is reduced to 1.3 Å as expected for a fully planar structure. Figure 2f shows an STM image of this new phase with a superimposed schematic model of the fully cyclodehydrogenated network. Good agreement is observed between the STM image and the model. Furthermore, imaging the unoccupied density of states of the resulting cyclodehydrogenated network shows a fundamental change of the network appearance (see Figure S1 in Supporting Information). The new features showing up under such tunneling conditions allow for a precise determination of the monomer orientation inside the network, corroborating that N atoms are aligned along the intermolecular bonding direction (see Supporting Information for further details). These results clearly prove that SAC allows for the complete cyclodehydrogenation of monomer **1** with a nearly 100% yield, which cannot be obtained by traditional solution-based chemistry and which represents a much higher efficiency than that achievable by thermolysis.[24]

Monomer **2**, although closely related to monomer **1**, presents a different behavior due to its higher structural flexibility. Deposition of **2** on the clean Ag(111) surface held at 425 K gives rise to the type of structures shown in Figure 3a. First, it is possible to discern the expected 6-fold symmetry of the molecule (due to the six phenyl rings attached to the central borazine ring). Six intramolecular features coincide with the position of the six phenyl rings, as clearly inferred by the comparison of the STM image with the schematic model shown in Figure 3e. The apparent height of these phenyl rings is 1.6 Å, clearly larger than the 1.3 Å obtained for the fully planar molecule, and reflects the expected nonzero dihedral angle that minimizes steric repulsion. The distance between adjacent molecules (~12.5 Å) indicates formation of covalent C−C bonds already at this temperature, in contrast to what is observed for monomer **1**. This different behavior can be attributed to

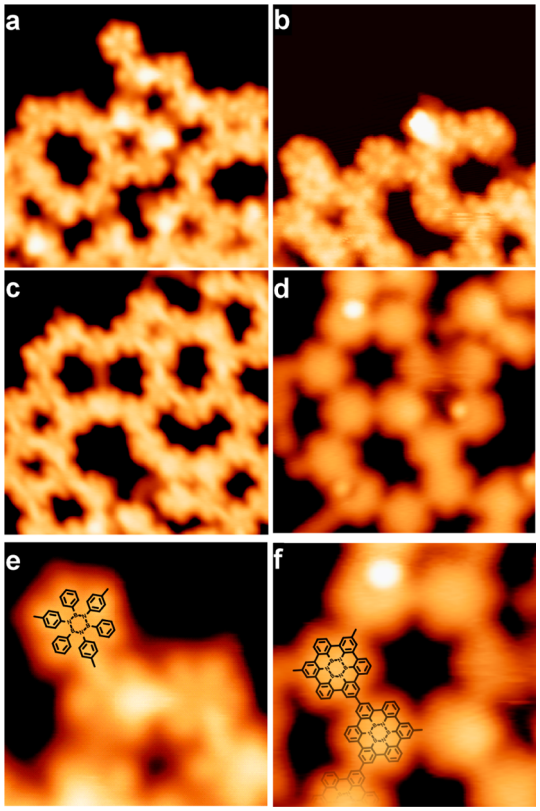

Figure 3. STM images of monomer 2 deposited on the clean Ag(111) surface after annealing to 425 K (a), (90 Å × 90 Å, I = 100 pA, U = −1.0 V); 475 K (b), (90 Å × 90 Å, I = 80 pA, U = −1.2 V, T = 77 K); 525 K (c) (90 Å × 90 Å, I = 250 pA, U = −1.0 V); and 625 K (d), (60 Å × 60 Å. I = 250 pA, U = −0.3 V). Annealing up to 575 K (a−c) results in the formation of the covalently bonded network without any signs of intramolecular cyclodehydrogenation. Further annealing to 625 K then yields the fully cyclodehydrogenated network (d). (e) High-resolution STM image of the network obtained after annealing at 425 K, with a schematic molecular model superimposed (38 Å × 38 Å, I = 100 pA, U = −1.0 V). (f) High-resolution STM image of the fully cyclodehydrogenated network obtained after annealing to 625 K. A good agreement with the scaled schematic molecular model is observed (38 Å × 38 Å, I = 250 pA, U = −0.3 V).

a decrease in the C−C bond formation energy barrier induced by the higher flexibility of monomer **2**.

If the system is postannealed at 475 K, no differences are observed with respect to 425 K (Figure 3b). Molecules preserve the same apparent height and separation with respect to their neighbors, as well as their 6-fold symmetry, thus indicating no substantial changes. The same is true after annealing at 525 K (Figure 3c) and 575 K (not shown). However, annealing the sample at 625 K yields the expected transition from a 6-fold molecular symmetry to a homogeneous appearance (with no internal structure), as shown in Figure 3d. Similar to the observations made for monomer **1**, the disappearance of the intramolecular features is accompanied by a decrease in apparent height from 1.6 to 1.35 Å. On the other hand, the transition from the initial precursor to the final fully cyclodehydrogenated BN-HBC unit takes place all at once, with no detectable intermediate states, opposed to what is observed for monomer **1**. This result can be rationalized in terms of different cyclodehydrogenation energy barriers as will be shown below. According to the results obtained for **1**, the temperature necessary for dehydrogenative C−C bond formation between two "wings" is around 525 K. This value is much lower than the temperature necessary to overcome the cyclodehydrogenation barrier for the formation of a "wing" in **2**, which is around 625 K. This means that once monomer **2** has enough thermal energy to overcome the energy barrier of the first cyclodehydrogenation step, the second one will be triggered immediately and the molecule directly undergoes complete cyclodehydrogenation.

To elaborate a detailed picture of the cyclodehydrogenation paths of **1** and **2**, we have computed the cyclodehydrogenation energy barriers for both monomers (see Computational details). Cyclodehydrogenation can be understood to proceed in four steps: (i) the outer molecular "wings" of the adsorbed molecules adopt a more coplanar geometry due to van der Waals interaction with the metallic surface, which already induces a certain degree of strain in the C−H bonds. Additional C−H bond weakening and final formation of the new covalent C−C bonds between neighboring "wings" is obtained upon annealing. The two H atoms attached to the bonding C atoms are pushed toward the surface and the vacuum, respectively. (ii) The H atom facing the surface is catalytically cleaved from the C atom (see **State 1** panels in Figure 4). (iii) The second H atom shifts to the neighboring C edge atom where it again adopts an sp^3 geometry with the other H atom being forced to approach the surface (**State 2** panels). (iv) The H atom facing the surface is again catalytically cleaved, thus leading to the final cyclodehydrogenated structure (**FS** panels). A similar path has been determined for the case of graphene nanoribbons.[30] The upper panel in Figure 4 shows the calculated energy barriers for the cyclodehydrogenation process (blue and red curves for monomers **1** and **2**, respectively). The highest energy barrier in the whole sequence corresponds to the transition between **IS** and **State 1**, *i.e.*, C−C bond formation and first H atom release. Furthermore, a clear energy difference for this transition is observed between the two monomers (∼0.9 eV), the barrier being higher for **2**, in good agreement with the experimental results. Once the C−C bond has been formed and the first H atom is released (**State 1**), the energy barriers are very small or even negligible until the **FS** is reached. It is worthy to note that the **FS**s for both monomers are different, but closely related: **FS** of monomer **2** is similar to the **IS** of **1**, while **FS** of monomer **1** is close to complete cyclodehydrogenation. Thus, if enough thermal energy to overcome the first energy barrier is supplied to monomer **2**, there will be no energetic limitations for the system to undergo full cyclodehydrogenation since

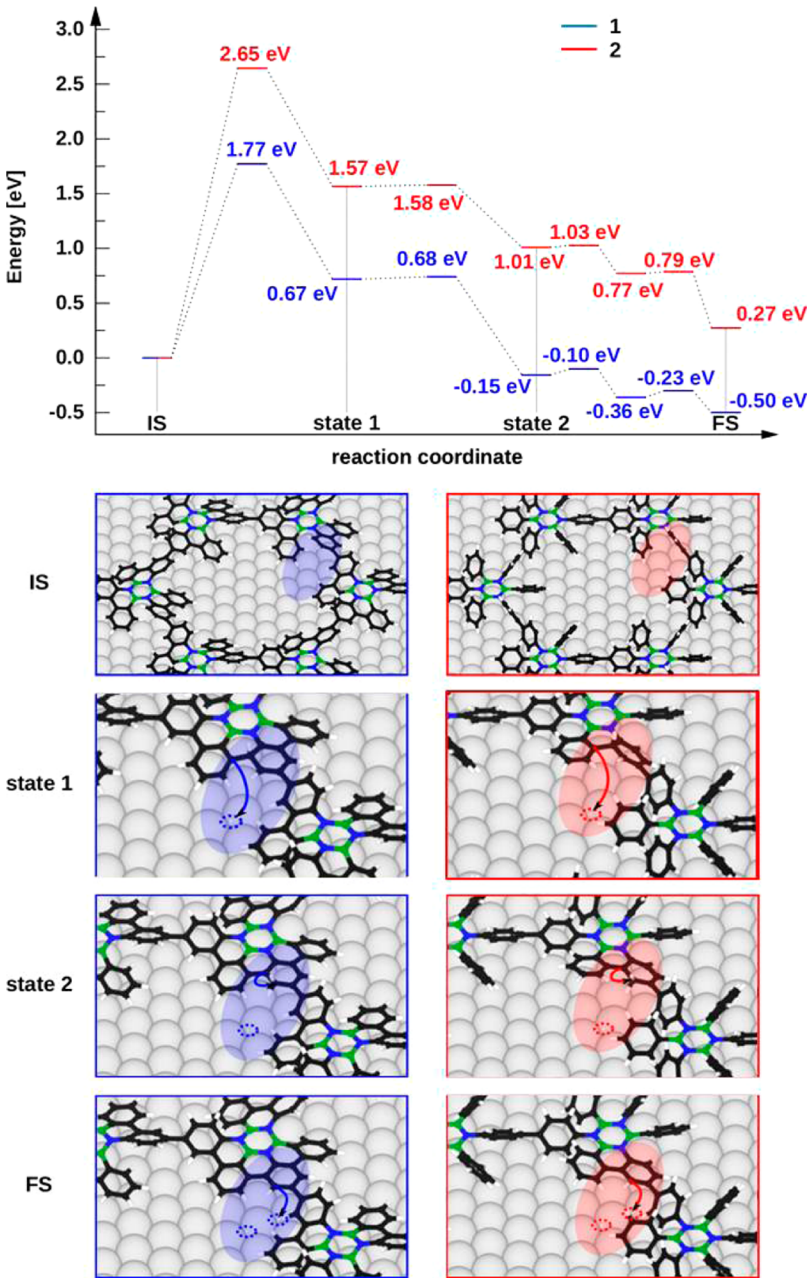

Figure 4. Energy barriers for the first cyclodehydrogenation steps computed for both monomers: formation of the new C−C bond and release of the two H atoms. Top panel: Energy barriers for monomers 1 and 2. IS and FS refer to Initial State and Final State, respectively. Energy levels have been aligned at IS. Lower panel: Schematic representation of the steps involved in the cyclodehydrogenation. Left (blue) and right (red) refer to monomers 1 and 2, respectively. Gray, black, blue, green, and white correspond to Ag, C, N, B, and H atoms, respectively.

energy barriers for monomer **1** are much lower. This rationalizes the absence of partially cyclodehydrogenated intermediates for monomer **2**.

Heretofore it has been shown that both monomers, **1** and **2**, give rise to the same final product from the molecular point of view. Furthermore, due to on-surface aryl−aryl coupling, both of them successfully yield the formation of BN-substituted porous graphene with atomically precise BN/C boundaries. Panels a and b of Figure 5 show two large-scale STM images of the final structures obtained upon complete cyclodehydrogenation of monomers **1** and **2**, respectively. Monomer **1** creates a well-ordered network with a clear prevalence of six-membered pores, while monomer **2** produces a low quality network with a much wider distribution in pore composition, as evidenced by the histogram shown in Figure 5c. Long range order is established during the intermolecular C−C bond formation step, when monomers are still in their initial state, *i.e.*, without any intramolecular cyclodehydrogenation. Therefore, the observed difference in long-range order must be associated with the different conformational flexibility

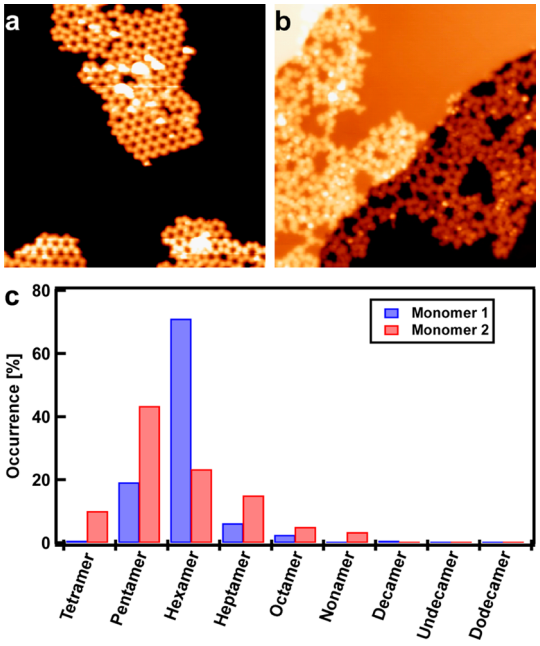

Figure 5. STM characterization of the long-range order of the fully cyclodehydrogenated networks obtained from monomers 1 (a) (500 Å × 500 Å, I = 500 pA, U = −1.0 V) and 2 (b) (400 Å × 400 Å, I = 100 pA, U = −1.2 V). (c) Statistical analysis of the number of monomers per network pore for both monomers.

of the precursor monomers. Whitelam *et al.* have recently shown that long-range order in networks composed of molecular building blocks is critically affected by two main factors, bond strength and flexibility.[31] Weak and rigid bonds yield a highly ordered network, while strong and flexible bonds give rise to disordered structures. Applied to the case presented here, the bond strength does not play a role because both monomers form the same type of bonds, *i.e.*, covalent C−C bonds. However, flexibility is the parameter determining the quality of the final network. Peripheral phenyl rings in monomer **2** form single bonds to the central borazine ring, which allows for a higher flexibility than in the case of monomer **1**, where the already formed C−C bond between each two peripheral phenyl rings implies that each "wing" is fixed to the borazine core by two C−C bonds. This explains why the stiffer monomer **1** yields the more ordered network (see Figure 5a), whereas the more flexible monomer **2** forms a rather disordered network (Figure 5b). This shows that, in addition to substrate-specific diffusion and coupling probabilities[32] (see Supporting Information for further details), molecular flexibility has a decisive influence on the long-range order of the resulting network.

CONCLUSIONS

We have shown that surface-assisted polymerization and subsequent cyclodehydrogenation of bromine-substituted borazines **1** and **2** allow for the fabrication of covalently interlinked BN-HBC networks on Ag(111). For **2**, complete cyclodehydrogenation is achieved at 625 K, whereas for the more rigid **1**, this temperature is reduced to 575 K due to a substantially lowered energy barrier for the initial C−C bond formation step, as confirmed by DFT calculations. In both cases, the same BN-HBC subunits are formed, as evidenced by STM. Comparison of high-resolution STM images and their corresponding DFT-based simulations clearly proves that the borazine ring is preserved in its original position and orientation, thus demonstrating that our bottom-up strategy allows for ultimate structural control over BN doping in heteroaromatic covalent networks. Regarding the long-range order of the BN-HBC network, we find a marked dependence on the flexibility of the precursor monomers during the polymerization step. The higher flexibility of **2** results in a wide distribution of intermolecular bond angles and correspondingly poor long-range order, whereas the more rigid **1** preferably forms six-membered pores, which are compatible with a high degree of long-range order. Our proof-of-concept study opens a door toward the design and synthesis of atomically precise BNC heterostructures such as 0D BNC "flakes", 1D BNC nanoribbons and 2D BNC layers or networks, with properties that may be tailored by adjusting the BN to C ratio. Certainly, our proposed on-surface synthetic approach is not deprived of challenges, like the direct growth onto technologically relevant substrates. However, recent advances in the postgrowth transfer of graphene-related nanostructures onto insulating materials[33,34] offer opportunities to exploit electronic and structural properties of the so-formed nanostructures in future applications.

METHODS

Experiments have been carried out in an ultrahigh vacuum system (base pressure below 10^{-10} mbar) equipped with a LT-STM (5 K, Omicron NanoTechnology, GmbH). Ag(111) single crystals (SPL) were cleaned by repeated Ar^+ sputtering (1.0 kV) and annealing (750 K) cycles until judged clean by STM. Both monomers were thermally sublimed from a 3-fold Kentax evaporator stabilized in temperature through a PID controller. A deposition rate of approximately 1 Å/min (determined by a quartz microbalance) was used during deposition (deposition temperatures of 490 and 440 K for monomer **1** and **2**, respectively). STM images were recorded in constant current mode. Unless otherwise stated, all STM images were recorded at 5 K. All temperatures expressed throughout the manuscript were measured with a pyrometer focused on the sample surface and aligned perpendicular to it (Optris, emissivity ε = 0.1).

First-principles calculations have been carried out within the framework of plane-wave DFT using the VASP 5.3 software package.[35,36] We have employed the generalized gradient approximation (GGA) using the PerdewBurke-Ernzerhof (PBE) exchange-correlation functional.[37] The projected augmented wave (PAW) method was used to describe the ion−core electron

interactions.[38,39] van der Waals interactions were included using the van der Waals density functional (vdW-DF),[40] as implemented in VASP 5.3 on top of GGA using the optB86b functional.[41] The Ag(111) surface has been modeled by three layered slabs separated by at least 15 Å of vacuum, and a p(8 × 8) surface unit cell has been used with a calculated lattice constant of 4.091 Å. All calculations have been done using "Gamma" (Γ) point only k-point integration and a 500 eV kinetic energy cutoff. The relatively high cutoff ensures convergence of the Ag lattice constant when computed with the vdW-DF. All structures have been relaxed until the forces acting on the atoms in the molecules and the uppermost layers of the slabs are smaller than 0.01 eV/Å. Transition-state calculations have been carried out using the nudged elastic band method (NEB). The number of images has been adjusted specifically for each transition-state calculation such that the tangent along the path is well described. Typically, 8 images have been used between each step of the reaction, *i.e.*, 24 images in total, and the structural optimization has been performed until the forces acting on the atoms are smaller than 0.05 eV/Å.

Conflict of Interest: The authors declare no competing financial interest.

Acknowledgment. We are grateful for the financial support from the European Research Council grant on NANOGRAPH, DFG Priority Program SPP 1459, Graphene Flagship (No. CNECT-ICT-604391), European Union Projects MoQuaS, the Office of Naval Research BRC Program, Deutsche Forschungsgemeinschaft and the Swiss National Science Foundation. Large-scale computations were performed at the Center for Computational Innovation (CCI) at Rensselaer.

Supporting Information Available: The Supporting Information is available free of charge on the ACS Publications website at DOI: 10.1021/acsnano.5b03895.

Monomers synthesis and characterization; orientation determination of the BN core by combination of STM and DFT (PDF)

REFERENCES AND NOTES

1. Méndez, J.; López, M. F.; Martín-Gago, J. A. On-Surface Synthesis of Cyclic Organic Molecules. *Chem. Soc. Rev.* **2011**, *40*, 4578–4590.
2. Otero, G.; Biddau, G.; Sánchez-Sánchez, C.; Caillard, R.; López, M. F.; Rogero, C.; Palomares, F. J.; Cabello, N.; Basanta, M. A.; Ortega, J.; et al. Fullerenes from Aromatic Precursors by Surface-Catalysed Cyclodehydrogenation. *Nature* **2008**, *454*, 865–868.
3. Amsharov, K.; Abdurakhmanova, N.; Stepanow, S.; Rauschenbach, S.; Jansen, M.; Kern, K. Towards the Isomer-Specific Synthesis of Higher Fullerenes and Buckybowls by the Surface-Catalyzed Cyclodehydrogenation of Aromatic Precursors. *Angew. Chem., Int. Ed.* **2010**, *49*, 9392–9396.
4. Rim, K. T.; Siaj, M.; Xiao, S.; Myers, M.; Carpentier, V. D.; Liu, L.; Su, C.; Steigerwald, M. L.; Hybertsen, M. S.; McBreen, P. H.; et al. Forming Aromatic Hemispheres on Transition-Metal Surfaces. *Angew. Chem., Int. Ed.* **2007**, *46*, 7891–7895.
5. Sánchez-Sánchez, C.; Martínez, J. I.; Lanzilotto, V.; Biddau, G.; Gómez-Lor, B.; Pérez, R.; Floreano, L.; López, M. F.; Martín-Gago, J. Á. Chemistry and Temperature-Assisted Dehydrogenation of C 60 H 30 Molecules on TiO 2 (110) Surfaces. *Nanoscale* **2013**, *5*, 11058–11065.
6. Pinardi, A. L.; Martínez, J. I.; JančaŖík, A.; Stará, I. G.; Star, I.; López, M. F.; Méndez, J.; Martín-Gago, J. Á. Sequential Formation of N-Doped Nanohelicenes, Nanographenes and Nanodomes by Surface-Assisted Chemical (cyclo) Dehydrogenation of Heteroaromatics. *Chem. Commun.* **2014**, *50*, 1555–1557.
7. Treier, M.; Pignedoli, C. A.; Laino, T.; Rieger, R.; Müllen, K.; Passerone, D.; Fasel, R. Surface-Assisted Cyclodehydrogenation Provides a Synthetic Route towards Easily Processable and Chemically Tailored Nanographenes. *Nat. Chem.* **2011**, *3*, 61–67.
8. Pinardi, A. L.; Otero-Irurueta, G.; Palacio, I.; Martinez, J. I.; Sanchez-Sanchez, C.; Tello, M.; Rogero, C.; Cossaro, A.; Preobrajenski, A.; Gómez-Lor, B.; et al. Tailored Formation of N-Doped Nanoarchitectures by Diffusion-Controlled on-Surface (Cyclo) Dehydrogenation of Heteroaromatics. *ACS Nano* **2013**, *7*, 3676–3684.
9. Björk, J.; Stafström, S.; Hanke, F. Zipping up: Cooperativity Drives the Synthesis of Graphene Nanoribbons. *J. Am. Chem. Soc.* **2011**, *133*, 14884–14887.
10. Sachdev, H.; Zahn, N.; Huch, V. Structural and Spectroscopic Properties of Aryl Substituted Aminoboranes as Model Compounds and Synthons for B/C/N Materials and New Fluorescent Systems. *Z. Anorg. Allg. Chem.* **2009**, *635*, 2112–2119.
11. Rubio, A. Hybridized Graphene: Nanoscale Patchworks. *Nat. Mater.* **2010**, *9*, 379–380.
12. Jariwala, D.; Srivastava, A.; Ajayan, P. M. Graphene Synthesis and Band Gap Opening. *J. Nanosci. Nanotechnol.* **2011**, *11*, 6621–6641.
13. Shinde, P. P.; Kumar, V. Direct Band Gap Opening in Graphene by BN Doping: Ab Initio Calculations. *Phys. Rev. B: Condens. Matter Mater. Phys.* **2011**, *84*, 125401.
14. Xu, B.; Lu, Y. H.; Feng, Y. P.; Lin, J. Y. Density Functional Theory Study of BN-Doped Graphene Superlattice: Role of Geometrical Shape and Size. *J. Appl. Phys.* **2010**, *108*, 073711.
15. Karamanis, P.; Otero, N.; Pouchan, C. Unleashing the Quadratic Nonlinear Optical Responses of Graphene by Confining White-Graphene (h-BN) Sections in Its Framework. *J. Am. Chem. Soc.* **2014**, *136*, 7464–7473.
16. Usachov, D.; Adamchuk, V. K.; Haberer, D.; Grüneis, A.; Sachdev, H.; Preobrajenski, A. B.; Laubschat, C.; Vyalikh, D. V. Quasifreestanding Single-Layer Hexagonal Boron Nitride as a Substrate for Graphene Synthesis. *Phys. Rev. B: Condens. Matter Mater. Phys.* **2010**, *82*, 075415.
17. Liu, Z.; Ma, L.; Shi, G.; Zhou, W.; Gong, Y.; Lei, S.; Yang, X.; Zhang, J.; Yu, J.; Hackenberg, K. P. In-Plane Heterostructures of Graphene and Hexagonal Boron Nitride with Controlled Domain Sizes. *Nat. Nanotechnol.* **2013**, *8*, 119–124.
18. Levendorf, M. P.; Kim, C.-J.; Brown, L.; Huang, P. Y.; Havener, R. W.; Muller, D. A.; Park, J. Graphene and Boron Nitride Lateral Heterostructures for Atomically Thin Circuitry. *Nature* **2012**, *488*, 627–632.
19. Gao, Y.; Zhang, Y.; Chen, P.; Li, Y.; Liu, M.; Gao, T.; Ma, D.; Chen, Y.; Cheng, Z.; Qiu, X. Toward Single-Layer Uniform Hexagonal Boron Nitride−graphene Patchworks with Zigzag Linking Edges. *Nano Lett.* **2013**, *13*, 3439–3443.
20. Sutter, P.; Cortes, R.; Lahiri, J.; Sutter, E. Interface Formation in Monolayer Graphene-Boron Nitride Heterostructures. *Nano Lett.* **2012**, *12*, 4869–4874.
21. Ci, L.; Song, L.; Jin, C.; Jariwala, D.; Wu, D.; Li, Y.; Srivastava, A.; Wang, Z. F.; Storr, K.; Balicas, L. Atomic Layers of Hybridized Boron Nitride and Graphene Domains. *Nat. Mater.* **2010**, *9*, 430–435.
22. Kim, S. M.; Hsu, A.; Araujo, P. T.; Lee, Y.-H.; Palacios, T.; Dresselhaus, M.; Idrobo, J.-C.; Kim, K. K.; Kong, J. Synthesis of Patched or Stacked Graphene and hBN Flakes: A Route to Hybrid Structure Discovery. *Nano Lett.* **2013**, *13*, 933–941.
23. Gong, Y.; Shi, G.; Zhang, Z.; Zhou, W.; Jung, J.; Gao, W.; Ma, L.; Yang, Y.; Yang, S.; You, G. Direct Chemical Conversion of Graphene to Boron-and Nitrogen-and Carbon-Containing Atomic Layers. *Nat. Commun.* **2014**, *5*, 3193.
24. Krieg, M.; Reicherter, F.; Haiss, P.; Ströbele, M.; Eichele, K.; Treanor, M.-J.; Schaub, R.; Bettinger, H. F. Construction of an Internally B3N3-Doped Nanographene Molecule. *Angew. Chem., Int. Ed.* **2015**, *54*, 8284.
25. Biswas, S.; Müller, M.; Tönshoff, C.; Eichele, K.; Maichle-Mössmer, C.; Ruff, A.; Speiser, B.; Bettinger, H. F. The Overcrowded Borazine Derivative of Hexabenzotriphenylene Obtained through Dehydrohalogenation. *Eur. J. Org. Chem.* **2012**, *2012*, 4634–4639.
26. Tönshoff, C.; Müller, M.; Kar, T.; Latteyer, F.; Chassé, T.; Eichele, K.; Bettinger, H. F. B3N3 Borazine Substitution in

Hexa-Peri-Hexabenzocoronene: Computational Analysis and Scholl Reaction of Hexaphenylborazine. *ChemPhysChem* **2012**, *13*, 1173–1181.
27. Müller, M.; Maichle-Mössmer, C.; Sirsch, P.; Bettinger, H. F. Is There B-N Bond-Length Alternation in 1, 2:3, 4 5, 6-Tris (biphenylylene) Borazines? *ChemPlusChem* **2013**, *78*, 988–994.
28. Eichhorn, J.; Strunskus, T.; Rastgoo-Lahrood, A.; Samanta, D.; Schmittel, M.; Lackinger, M. On-Surface Ullmann Polymerization *via* Intermediate Organometallic Networks on Ag (111). *Chem. Commun.* **2014**, *50*, 7680–7682.
29. Bieri, M.; Blankenburg, S.; Kivala, M.; Pignedoli, C. A.; Ruffieux, P.; Müllen, K.; Fasel, R. Surface-Supported 2D Heterotriangulene Polymers. *Chem. Commun.* **2011**, *47*, 10239–10241.
30. Blankenburg, S.; Cai, J.; Ruffieux, P.; Jaafar, R.; Passerone, D.; Feng, X.; Müllen, K.; Fasel, R.; Pignedoli, C. A. Intraribbon Heterojunction Formation in Ultranarrow Graphene Nanoribbons. *ACS Nano* **2012**, *6*, 2020–2025.
31. Whitelam, S.; Tamblyn, I.; Haxton, T. K.; Wieland, M. B.; Champness, N. R.; Garrahan, J. P.; Beton, P. H. Common Physical Framework Explains Phase Behavior and Dynamics of Atomic, Molecular and Polymeric Network Formers. *Phys. Rev. X* **2014**, *4*, 011044.
32. Bieri, M.; Nguyen, M.-T.; Groening, O.; Cai, J.; Treier, M.; Aït-Mansour, K.; Ruffieux, P.; Pignedoli, C. A.; Passerone, D.; Kastler, M.; et al. Two-Dimensional Polymer Formation on Surfaces: Insight into the Roles of Precursor Mobility and Reactivity. *J. Am. Chem. Soc.* **2010**, *132*, 16669–16676.
33. Bennett, P. B.; Pedramrazi, Z.; Madani, A.; Chen, Y.-C.; de Oteyza, D. G.; Chen, C.; Fischer, F. R.; Crommie, M. F.; Bokor, J. Bottom-up Graphene Nanoribbon Field-Effect Transistors. *Appl. Phys. Lett.* **2013**, *103*, 253114.
34. Cai, J.; Pignedoli, C. A.; Talirz, L.; Ruffieux, P.; Söde, H.; Liang, L.; Meunier, V.; Berger, R.; Li, R.; Feng, X.; et al. Graphene Nanoribbon Heterojunctions. *Nat. Nanotechnol.* **2014**, *9*, 896–900.
35. Kresse, G.; Furthmüller, J. Efficiency of Ab-Initio Total Energy Calculations for Metals and Semiconductors Using a Plane-Wave Basis Set. *Comput. Mater. Sci.* **1996**, *6*, 15–50.
36. Kresse, G.; Furthmüller, J. Efficient Iterative Schemes for Ab Initio Total-Energy Calculations Using a Plane-Wave Basis Set. *Phys. Rev. B: Condens. Matter Mater. Phys.* **1996**, *54*, 11169.
37. Perdew, J. P.; Burke, K.; Ernzerhof, M. Generalized Gradient Approximation Made Simple. *Phys. Rev. Lett.* **1996**, *77*, 3865.
38. Blöchl, P. E. Projector Augmented-Wave Method. *Phys. Rev. B: Condens. Matter Mater. Phys.* **1994**, *50*, 17953.
39. Kresse, G.; Joubert, D. From Ultrasoft Pseudopotentials to the Projector Augmented-Wave Method. *Phys. Rev. B: Condens. Matter Mater. Phys.* **1999**, *59*, 1758.
40. Dion, M.; Rydberg, H.; Schröder, E.; Langreth, D. C.; Lundqvist, B. I. Van Der Waals Density Functional for General Geometries. *Phys. Rev. Lett.* **2004**, *92*, 246401.
41. Klimeš, J.; Bowler, D. R.; Michaelides, A. Van Der Waals Density Functionals Applied to Solids. *Phys. Rev. B: Condens. Matter Mater. Phys.* **2011**, *83*, 195131.